International Journal of Innovation in Science and Mathematics
Volume 5, Issue 3, ISSN (Online): 2347–9051

Karman Turbulence Model Simulations of Supersonic Open-Cavity Flows

Pinchukov V.I.
In-te of Computational Technologies, Siberian division of Russian Academy of Sc., Novosibirsk, Russia
Corresponding author email id: pinchvi@ict.nsc.ru

Date of publication (dd/mm/yyyy): 12/06/2017

Abstract **– Results of numerical investigations of self-oscillatory cavity flows are represented. Two-dimensional Reynolds-averaged Navier-Stocks equations coupled with the algebraic Karman turbulence model are solved by an implicit third order Runge-Kutta scheme. The turbulent viscosity is defined by the Prandtl formulae, which deals with the turbulent length scale calculated on the base of the generalized Karman formulae. Steady flow, resulted from interaction of two supersonic parallel flows are modeled to check convergence to a steady state solution. Calculations of the low Mach number flow near plain surface are carried out to prove existence of logarithmic part in the boundary layer profile. A turbulent open cavity flow at Mach 1.5 and 2.5 is modeled to study the flow physics. Results of calculations are compared with results of other computations.**

Keywords **– High Resolution Methods, Reynolds-Averaged-Navier-Stocks Equations, Self-Oscillatory Flows.**

NOMENCLATURES

1. Pressure P ,
2. Density ρ,
3. Mach number M,
4. Viscosity μ,
5. Vorticity w,
6. Length scale z,
7. Specific heat ratio γ,
8. Distance to solid surface d_w ,
9. Physical space variables x, y,
10. Transformed variables ξ , η.

I. INTRODUCTION

Progress in CFD studies of self-oscillatory compressible flows makes natural and possible next step of investigations – CFD search for new unsteady flows. This search is connected with numerous calculations of diverse flows. So, economical and universal turbulence model is required. Classical algebraic models [1],[2] are economical and relatively simple, but are not universal. Recent paper is devoted to development and applications of the algebraic model of turbulence, constructed in [3] on the base of the generalized Karman formulae for the turbulent length scale. This generalization is performed to extend applicability of the Karman formulae to regions beyond boundary layers. Above of universality, additional distinguishing feature of the Karman model is usage of averaging. It should be memorized that highest solution derivatives in every space variable and time should be considered to define type of equations. If turbulent viscosity depends on derivatives of solution, the type of RANS may differ from the parabolic type of NS equations. To avoid this effect the averaging is used in the Karman model.

Self-oscillatory cavity flows may contain complicated structures of shear layers and shock waves, generation of cavity flow oscillations is resulted from interactions of numerous flow elements. So CFD study of these flows may be used to check the turbulence model. Classification of unsteady cavity flows may be performed according to geometry (open cavity flows and closed cavity flows) and according to physics of flows. The feedback mechanism is divided into fluid-dynamic and fluid resonant in [4]. Incompressible flows such as low Mach number air cavity flows are classified as fluid-dynamic oscillatory. The self-sustaining cavity oscillations in compressible flows at high Mach numbers are classified as fluid-resonant oscillations. Other reasons for classification are suggested in [3],[5]-[6]. Generation of self-oscillations are supposed to be resulted from resonance interactions of "active" flow elements, namely, elements, increasing disturbances. Contact discontinuities and intersection points (lines in 3D case) of shock waves with shock waves or shock waves with contact discontinuities compose sets of flow active elements. According to this self-oscillation mechanism, classification of unsteady flows depends on sets of flows "active" elements. Subsonic flows may contain only elements of the first type, namely, contact discontinuities. So, subsonic cavity flows produce self-oscillations as a result of interactions of two or more contact discontinuities. Supersonic cavity flows contain also elements of the second type, namely, intersection points, mentioned above, which may be involved to interactions, producing flow oscillations.

Investigations of unsteady cavity flows are concerned for various aspects. For example, the mode switching for the cavity flows is studied in [7]-[9]. Active and passive flow control techniques are considered in [10]-[13]. The noise generation physics of the unsteady cavity flow is investigated in [14]-[17].

II. THE KARMAN MODEL OF TURBULENCE

The initial Karman model [3] is modified significantly here. Namely, two control parameters are used instead of one parameter, generalized Karman formula is changed, averaging is used twice and new weight function of averaging is applied. The Karman algebraic model of turbulence deals with the Prandtl formulae $\mu_{tur} = \rho|w|z^2$, where w is vorticity, ρ is density, $z=kl$, l is the turbulent length scale, k=0.4 is the Karman coefficient. This formulae is applied in classical Cebeci-Smith and Baldween-Lomax models [1]-[2], where the length scale is

defined as a distance to a solid wall. Another definition of the length scale is used here. The Karman formulae

$z=k\,\partial u/\partial y\,/(\partial^2 u/\partial y^2)$

is applied in the theory of a turbulent boundary layer. The idea of recent model is to use generalization of this formulae:

$l \approx |w(x,y)|/|\nabla w(x,y)|$, (1)

where $\nabla w(x,y)$ – vector $(\partial w/\partial x,\ \partial w/\partial y)$,

$|\nabla w(x,y)| = [(\partial w/\partial x)^2 + (\partial w/\partial y)^2]^{1/2}$, w - vorticity.

Of course, the formulae (1) gives bad results in regions with "small" values of $|\nabla w(x,y)|$ and so should be modified. Next procedure of turbulent viscosity calculations is used here:

$l=|w|/[\underline{|\nabla w|^2} + \delta(|\nabla u|^2 + |\nabla v|^2)/\mathrm{Det}]^{1/2}$, (2)

$z=\min\{l/[(1+l^4/\lambda^4)(1+l^2(l^2-0.7c^2)^2/c^6)]^{1/4}, d_w\}$, (3)

$\mu_{tur} = \underline{\rho |w| (kz)^2}$, (4)

λ, c - control parameters, u,v – velocity components, d_w – distance to a solid surface, δ =0.0001- the coefficient, providing regularity of written above formulas in the case grad w $\approx$ 0,

$\mathrm{Det}=\partial x/\partial\xi \times \partial y/\partial\eta - \partial x/\partial\eta \times \partial y/\partial\xi$, ξ, η – transformed variables. The geometrical parameter c should be equal approximately to a maximal width of shear layers or boundary layers, parameter $\lambda < c$ allows to vary "level" of turbulence. To make the formulae (3) more clear the main expression of this formulae should be rewritten as a multiplication of two factors,

$l/[(1+l^4/\lambda^4)]^{1/4}$ and $1/[(1+l^2(l^2-0.7c^2)^2/c^6)]^{1/4}$.

First factor approximates the Karman formulae in regions with small values of the relation l/λ. This factor increases asymptotically till the value $l=\lambda$ as l increases. The second factor is approximately equal to 1 in the interval $0< l < c$, then this factor quickly decreases and tends to the zero limit as l increases. The turbulent length scale decreasing is intended to provide low level of the turbulent viscosity inside of circulation zones. Underlined expressions are averaged expressions in formulas (2)-(5), the averaging procedure consists of two steps

$$\underline{f_1} = \int_{-m\Delta x}^{m\Delta x} f_1(x+\varsigma,y)\,\Omega(m\Delta x,\varsigma)\,d\varsigma, \quad (5)$$

$$\underline{f} = \int_{-m\Delta y}^{m\Delta y} f_1(x,y+\varsigma)\,\Omega(m\Delta y,\varsigma)\,d\varsigma, \quad (6)$$

$$\Omega(\varepsilon,\varsigma) = (1.2-\varsigma^2/\varepsilon^2) \Big/ \int_{-\varepsilon}^{\varepsilon} (1.2-\varsigma^2/\varepsilon^2)\,d\varsigma.$$

It should be noted, RANS have parabolic type, if turbulent viscosity does not depend on first or higher derivatives of solution functions. To eliminate dependence of turbulent viscosity (1)-(4) on first and second derivatives, the averaging procedure (5)-(6) is used. This procedure provides "smoothing" of turbulent viscosity, consequently, improves convergence to steady state solutions and prevents false unsteadiness. The most dangerous expression, containing second derivatives - $|\nabla w|^2$ – is averaged really twice, namely, averaging is used in formulas (2) and (4), while only final averaging was used in the initial model [3]. It allows to decrease averaging region and to use the integer parameter m=4 (see form. (5)-(6)) instead of m=7 [3] and, consequently, to improve resolution of the recent approach. Averaging is divided into two steps (5)-(6) to diminish the computational cost of the procedure.

The purpose of usage of this model is to find flows, which keep unsteady regimes while the control parameter λ is increasing, but remains much less then geometrical lengths of problems. This turbulence model may be considered as a tool to simulate approximately the turbulent dissipation influence on solutions of NS equations.

III. Test Problems

The supersonic flow resulted from interaction of two parallel uniform streams (see fig. 1) is calculated on the base of Euler equations and RANS equations coupled with the written above turbulence model. The flow is defined by upper stream parameters $p^u=1$, $\rho^u=1$, $M^u=2.4$ and down stream parameters $p^d=0.25$, $\rho^d=0.5$, $M^d=4$. The 180×135 grid is used. Fig. 1 shows the density distribution in the case $\mu_{tur}=0$.

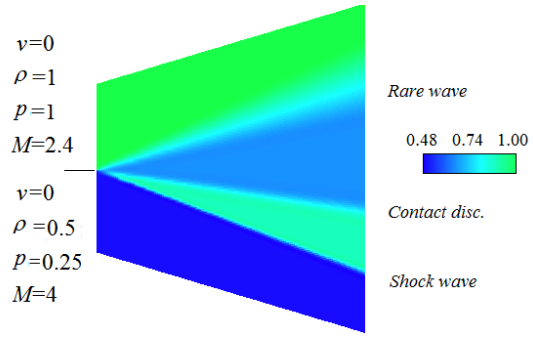

Fig. 1. Interaction of two ideal parallel streams, the density distribution

Fig. 2a, 2b represent results of flow calculations for the turbulent case. Karman model parameters c=0.075L (L - the left boundary size), λ=.05L are used. Turbulent Reynolds number $Re=L\,u^d\rho^d/\max_{ik}(\mu_{tur})$ of 88 is

resulted. Calculations are carried out for CFL number 1.38. Fig. 2a shows convergence histories, 1- the ideal case μ_{tur}=0, 2 – the turbulent case, 3 – turbulent viscosity is calculated without averaging.

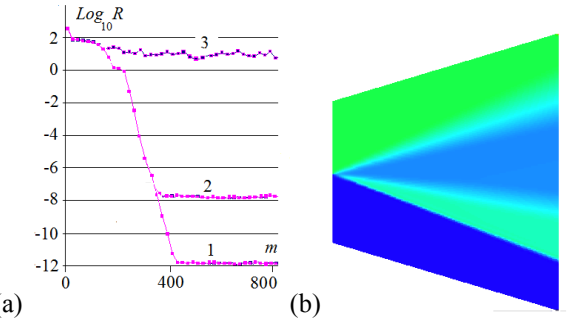

(a) (b)

Fig. 2. Supersonic streams interaction, a - convergence histories, b – the turbulent density distribution.

So, convergence histories show, that averaging is important part of the recent turbulent model since averaging provides convergence to a steady state solution. Fig 2b shows the turbulent flow density distribution. If to compare figs. 1 and 2b, difference is seen only in the zone of contact discontinuity. Fig. 2a demonstrates quick convergence to a steady state solution of the method [18] for the CFL number 1.38. But since large CFL numbers may lead to increasing of computation errors in the case of unsteady flows, recent investigations, written below, are carried out for CFL numbers within limits 0.5 – 1.

The low Mach number 2D flow near plane surface is calculated with usage of the Karman turbulence model. Fig. 3 shows the 45 × 18 mesh (the compression $\Delta x^{max}/\Delta x^{min} \approx \Delta y^{max}/\Delta y^{min} \approx 10$). The domain length d is equal to 1.75h.

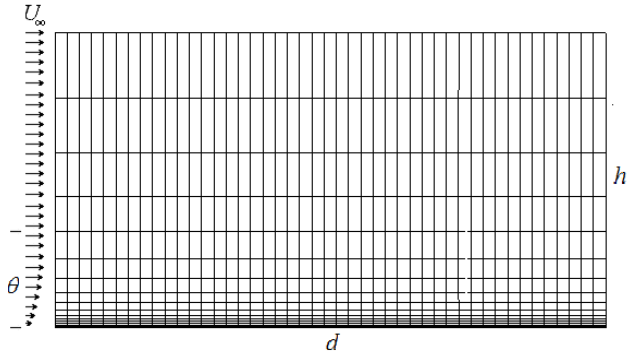

Fig. 3. The computational domain, the 45×18 mesh.

Boundary conditions for computations are no-slip adiabatic wall on the plane solid surface, extrapolations on the outflow boundary, prescribed variables on the inflow edge. Namely, dimensionless inflow pressure and density are 1, the vertical velocity v is 0, the horizontal velocity is $u = M_\infty \sqrt{\gamma} \sin(s\pi/2)$ if $s=y/\theta \le 1$, $u = M_\infty \sqrt{\gamma}$ if $s=y/\theta>1$, γ=1.4 – the specific heat ratio, θ - the initial boundary layer thickness, θ=0.75h. Calculations are carried out for flow conditions M_∞=0.3, μ_∞=1.3e-6. Mentioned above grid compression does not provide resolution of the laminar sublayer for this value of the physical viscosity. So, influence of turbulent viscosity on flow fields is dominant. Karman model parameters are chosen as c=0.9h, λ=0.6h. The 451×181 mesh is used. The turbulent Reynolds number Re = $\rho_\infty u_\infty \theta / /max_{ik}(\mu_{tur})$ =101 is resulted.

Fig. 4 shows inflow and outflow velocity profiles. Since low value of inflow Mach numbers M_∞=0.3 and adiabatic wall condition result small compressibility of the flow, the logarithmic part of velocity profile near the wall should be formed. Really, the nearly rectilinear part of the outflow logarithmic profile is seen in fig. 4.

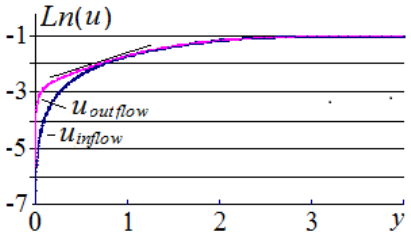

Fig. 4. Velocity profiles near the plain surface.

IV. The Computational Cavity Flow Model

The implicit conservative Runge-Kutta scheme [18] is employed here with some modifications. The initial method [18] is implemented in a computer code for sufficiently smooth curvilinear coordinate transformations $x=x(a,b)$, $y=y(a,b)$, mapping the unit square in the plane of variables a,b to a curvilinear quadrangle in the plane of physical variables x, y. Within this approach, it is difficult to obtain satisfactory meshes for complicated physical domains. For that reason, a special version of the code is developed for the case when functions $x=x(a,b)$, $y=y(a,b)$ perform mapping of the unit square with excisions $\{0\le a\le a_0, 0\le b\le b_0\}$, $\{a_1\le a\le 1, 0\le b\le b_1\}$ to a curvilinear quadrangle with curvilinear quadrangular excisions (see fig. 5). This version allows carrying out calculations, described below, without dividing complicated domains into subdomains. Both recent method and the method [18] are third order (viscous terms are approximated with the second order).

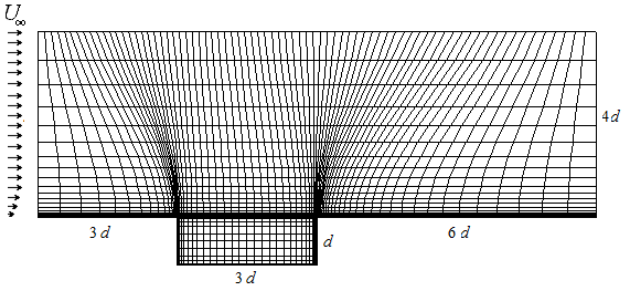

Fig. 5. The cavity computational domain, the 75×30 mesh.

Fig. 5 represents schematically the cavity geometry and the mesh (the mesh compression $\Delta x^{max} / \Delta x^{min} \approx \Delta y^{max} / \Delta y^{min} \approx 15$ is used). The flow geometry is defined by parameters d=5.5mm (the cavity depth, see fig. 5), L=16.5mm (the cavity length), the numerical region above cavity has the height of 22mm and the length of 60mm. This cavity flow is tested numerically with flow field conditions M_∞=1.5 or M_∞=2.5, θ_m= 0.417mm (the momentum thickness of the boundary layer on the inflow edge). Boundary conditions for computations are no-slip adiabatic wall on solid surfaces, extrapolations on the outflow boundaries, prescribed variables on the inflow edge. Namely, dimensionless pressure and density are 1, the vertical velocity v is 0, the horizontal velocity is u= $M_\infty \sqrt{\gamma}\,(2\sqrt{s}$ -s) if s=y/$\theta \le 1$, $u = M_\infty \sqrt{\gamma}$ if s=y/θ >1, γ=1.4 – the specific heat ratio, θ - initial boundary thickness. Boundary thickness θ is chosen as $\theta = \theta_m$ 30/13=0.962mm to provide the mentioned above momentum thickness value θ_m = 0.417mm.

Naturally, numerical calculations deal with dimensionless variables. These variables are defined as result of normalizations of initial variables by ambient parameters or the cavity depth d: p_∞ - for pressure, ρ_∞ - for a density, $\sqrt{p_\infty/\rho_\infty}$ - for a velocity, d – for space variables, $d/\sqrt{p_\infty/\rho_\infty}$ - for time. Calculations are carried out for normalized physical viscosity μ_{norm} = μ_∞ /[$d\rho_\infty \sqrt{p_\infty/\rho_\infty}$] =2.2e-6. Mentioned above grid compression does not provide resolution of the laminar sublayer for this value of physical viscosity. The turbulent viscosity influence on the flow fields is dominant in this case.

V. Results and Discussion

Fig. 6 shows the density distribution for the M_∞ =1.5 cavity flow. Karman model parameters c=0. 9d, λ=.06d are used. The 751 × 531 mesh is applied (quadrangular excisions contain 151×101 and 301×101 points, see fig. 5).

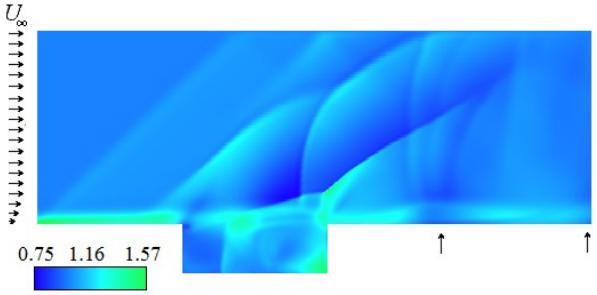

Fig. 6. The density distribution in the M_∞ =1.5 cavity flow

Fig. 7 show cavity bottom pressure histories at x_1=0.33 and x_2 =2.33 points.

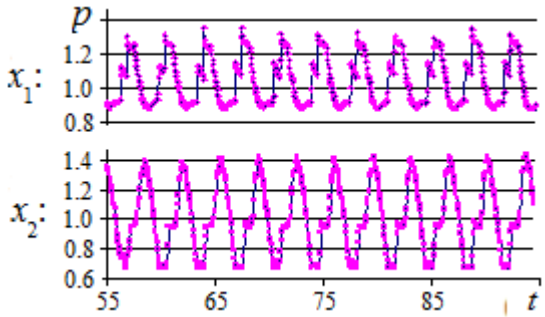

Fig. 7. Bottom pressure histories at x_1=0.33 and x_2 =2.33 points.

It may be seen that these histories are nearly periodical with the T=3.57 period. To show the flow dynamics through this time period density distributions at time moments $t=t_0+nT/4$, n=1…4, t_0 =95.0, T=3.57, are represented in figs. 8(a)-8(d).

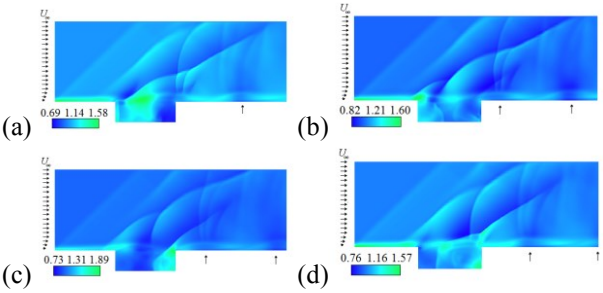

Fig. 8. Density distributions, (a) – t=t_0 +T/4,(b) – -t=t_0 +T/2, (c) - t=t_0 +3T/4, (d) – t=t_0 +T.

It is easy to see that fig. 6, which shows the density distribution at the time moment t= t_0 =90.0, and fig. 8(d) are like, so these figs. show nearly periodical dynamics of the considered unsteady flow.

Mass and momentum exchange between the free stream and the enclosed flow occurs across the open cavity top boundary. Unsteady mass ejection and entrainment at the downstream cavity edge may be seen in figs. 6, 8(a)-8(d). Vortexes positions are signed by arrows in these figs. During the mass ejection phase, a vortex leaves the cavity and is convected downstream, parallel to the free stream.

Time histories of the flow pressure at x_1=0.33 and x_2=2.33 points are used to form the time averaged sound pressure level $\overline{SPL}$, which is computed by the equation

$$\overline{SPL} = 20 \operatorname{Log}_{10} (\Delta p / p_{ref}), \; p_{ref} = 20\text{mkPa}/p_\infty,$$

where

$$\Delta p = \sqrt{\overline{p'^2}}, \quad \overline{p'^2} = \sum_n (p_n - \overline{p})^2 / N,$$

p_∞=101325Pa (air pressure under normal conditions) is used since dimensionless variables are dealt here. The time averaged $\overline{SPL}$ of 177.1Db is resulted for the x_1=0.33 point and $\overline{SPL}$ of 181.7Db is resulted for the x_2=2.33 point. These values may be compared with the $\overline{SPL}$ of 171Db at the x_1 point and the $\overline{SPL}$ of 176Db at the x_2 point, which may be defined approximately from graphs, presented in [15].

Fig. 9 shows the density distribution, calculated for the flow condition M_∞=2.5. Mass exchange between the free stream and the enclosed flow is not observed in this flow.

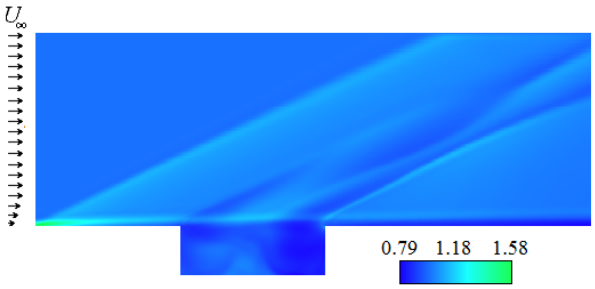

Fig. 9. The density distribution, M_{jet}=2.5.

Fig. 10 shows cavity flow pressure histories at x_1=0.33 and x_2=2.33 points.

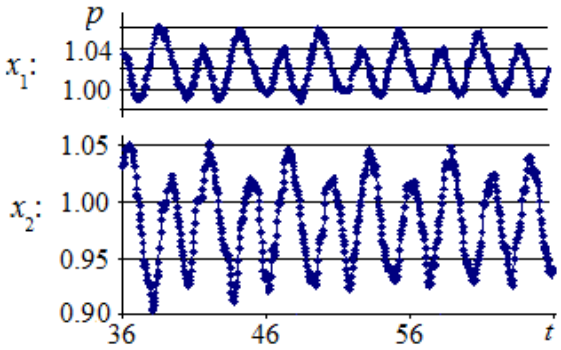

Fig. 10. Bottom pressure histories at x_1=0.33 and x_2=2.33 points.

The time averaged $\overline{SPL}$ of 159.9Db is resulted for the x_1=0.33 point and the $\overline{SPL}$ of 165.5Db is resulted for the x_2=2.33 point. These values may be compared with the $\overline{SPL}$ of 161Db at the x_1 point and the $\overline{SPL}$ of 163Db at the x_2 point, which may be defined from graphs, presented in [15].

It may be seen that these histories are nearly periodical with the T=5.89 period. To investigate flow dynamics in detail integration of RANS is performed for time interval [t=60, t=60+T]. It occurs that flow fields pictures for the first half of this time period are like to pictures for the second half period (but the first half period pressure history differs from the second half period history according to fig. 10). Figs. 11(a)-11(d) show streamlines pictures at time moments $t=t_0+nT/6$, n=3,…,6, t_0=60, T=5.89. Oscillations of the shear layer between the free stream and the enclosed flow are seen in these figs. The left part of the cavity contains changeable low velocity flow.

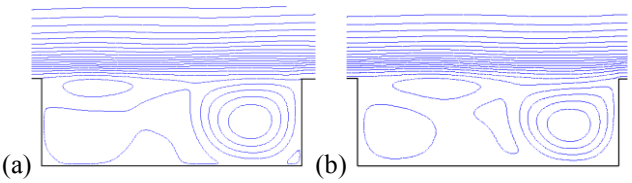

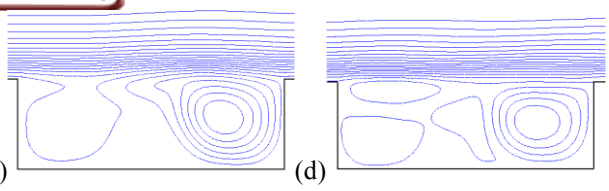

Fig. 11. Streamlines distributions, (a) – $t=t_o+T/2$,(b)- – $t=t_o+2T/3$, (c) - $t=t_o+5T/6$, (d) – $t=t_o+T$.

VI. Conclusions

Recent paper is devoted to development of the Karman model, suggested in [3]. Namely, resolution of the model is increased, the possibility to adapt model to any flow by choosing of control parameters becomes higher. This simple and universal model may be considered as a tool for fast numerous calculations of diverge flows, and, consequently, may be used at least in the first stage of a search for new self-oscillatory compressible flows. New unsteady flows may be investigated then by usage of more complicated and perfect turbulence models. Recent studies are a part of investigations, devoted to a numerical search for new self-oscillatory compressible flows, which is started in [5],[6] and is continued in [3].

To verify this model CFD studies of low Mach number flow near plane surface and supersonic cavity flow [15] are carried out here. The logarithmic low peace is observed in the velocity profile near a plane wall. Reasonable accord with cavity flow data [15] is demonstrated here.

References

[1] T. Cebeci, A. M. O. Smith, “Analysis of turbulent boundary layers”, Ser. In Appl. Math. & Mech., Vol. XV, 1974, Academic Press.

[2] B. S. Baldwin, H. Lomax, “Thin-layer approximation and algebraic model for separated turbulent flows”, AIAA Paper 78-257, 1978, Hu- ntsville, AL.

[3] V. I. Pinchukov, “Self-oscillatory flows near blunted bodies, giving off opposite jets: CFD study” Intern. J. of Engineering and Innova- tive Technology - Vol. 6, Issue 5, 2016, pp. 41-46.

[4] D. Rockwell, E. Naudascher, “Review of self-sustaining oscillations of flow past cavities”, ASME Journal of Fluids Engineering, 100, 1978, pp. 152-165.

[5] V. I. Pinchukov, “Numerical modeling of unsteady flows with tran- sient regimes”, Comput. Mathem. and Mathem. Physics, Vol. 49 (10), 2009, pp. 1844–1852.

[6] V. I. Pinchukov, “Modeling of self-oscillations and a search for new self-oscillatory flows”, Mathematical Models and Computer Simu-lations, Vol. 4(2), 2012, pp. 170–178.

[7] T. Yoshida, T. Watanabe, “Numerical simulation of flow over an open cavity with self-sustained oscillation mode switching”. Open Journal of Fluid Dynamics, 6, 2016, pp. 361-370.

[8] C. W. Rowley, T. Colonius, A.J. Basu, “On self-sustained oscilla-tions in two-dimensional compressible flow over rectangular cavi- ties”. Journal of Fluid Mechanics, 455, 2002, pp. 315-346. https: //doi.org/10.1017/S0022112001007534

[9] G. Rubio, W. De Roeck, M. Baelmans, W. Desmet, “Numerical ide- ntification of flow-induced oscillation modes in rectangular cavities using large eddy simulation”, International Journal for Numerical Methods in Fluids, 53, 2007, pp. 851-866. https://doi.org /10.1002/fld.1310

[10] S. Arunajatesan, C. Kannepalli, N. Sinha, “Analysis of control concepts for cavity flows”, 12th AIAA/CEAS Aeroacoustics Conference, 2006, AIAA Paper 2006 - 2427.

[11] C. W. Rowley, R. D. Williams, “Dynamics and control of high-Re-ynolds-number flow over open cavities”, Annu. Rev. Fluid Mech., Vol. 38, 2006, pp. 251–276.

[12] R. Nayyar, G. Barakos, K. Badcock, D. Kirkham, “Analysis and control of transonic cavity flow using DES and LES”, 2005, AIAA Paper 2005-5267.

[13] L. N. Cattafesta, O. Song, D. Williams, C. Rowley, F. S. Alvi, “Ac-tive control of flow-induced cavity oscillations”, Prog. Aerospace Sci., Vol. 44, 2008, pp. 479–502.

[14] G. Lilley, X. Zhang, A. Rona, “Progress in computational aeroaco-ustics in predicting the noise radiated from turbulent flows”, Inter-national Journal of Acoustics and Vibration 2 (1), 1997, pp. 3-10.

[15] A. Rona, “Self-excited supersonic cavity flow instabilities as aero-dynamic noise sources”, International Journal of Aeroacoustics, 5 (4), 2006, pp. 335-360.

[16] T. Colonius, “An overview of simulation, modeling, and active con-trol of flow acoustic resonance in open cavities”, Conference Paper 2001-0076, AIAA, 39th AIAA Aerospace Sciences Meeting & Exhibit, Reno, NV, USA, 2001.

[17] V. Theolis, “Advances in global linear instability analysis of nonparallel and three-dimensional flows”, Progress in Aerospace Sciences 39 (4), 2003, pp. 249-315.

[18] V.I. Pinchukov, “Numerical solution of the equations of viscous gas by an implicit third order Runge-Kutta scheme”, Comput. Mathem. and Mathem. Physics, Vol. 42(6), 2002, pp. 898-907.